IET Science, Measurement & Technology

WILEY

The Institution of Engineering and Technology

CASE STUDY OPEN ACCESS

Design and Development of a Magnetic Lead Screw With a Quasi-Halbach Array

Aly Ferreira Flores Filho[1] | Paulo Roberto Eckert[1] | David George Dorrell[2] | Davi von Mühlen Bertele[3] | Lucas Vinskoski[3]

[1]Graduate Programme in Electrical Engineering, Federal University of Rio Grande Do Sul, Porto Alegre, Brazil | [2]Department of Mechanical and Materials Engineering, University of Turku, Turku, Finland | [3]Department of Electrical Engineering, Federal University of Rio Grande Do Sul, Porto Alegre, Brazil

Correspondence: Aly Ferreira Flores Filho (aly.flores@ufrgs.br)

Received: 29 December 2025 | **Accepted:** 23 February 2026

ABSTRACT

This paper reports on a study of a novel magnetic lead screw (MLS) with a quasi-Halbach array and a rotor made of a soft magnetic composite (SMC). The proposed topology has an array formed from a helix of discretized pieces of permanent magnets (PMs) axially and radially magnetized in its slider. The rotor is formed from stacked discs of a soft magnetic composite and is experimentally tested. These are arranged to form the lead screw. Using finite element analysis (FEA) and static magnetic simulations, prototypes were assessed. The results show a good agreement in favour of the quasi-Halbach MLS with an SMC rotor.

1 | Introduction

Rotary-to-linear motion conversion is a fundamental requirement in a wide variety of engineering systems, ranging from precision industrial automation to high-force applications such as vehicle suspension actuators, wave energy converters, and aerospace mechanisms [1, 2]. Mechanical lead screws have long been the standard solution for these functions due to their ability to provide large forces, compact geometry, and mechanical simplicity. However, the reliance on direct mechanical contact between mating components introduces inherent limitations: friction, wear, lubrication requirements, noise, and reduced reliability under high-cycle operation. These constraints become increasingly problematic in modern applications demanding high efficiency, fast dynamics, and minimal maintenance.

To address these limitations, magnetically coupled transmission mechanisms have received growing attention. Among them, the MLS is an attractive alternative because it enables non-contact force transmission between the rotating and translating components [3, 4]. By replacing mechanical engagement with magnetic coupling, MLS devices eliminate friction between the slider and rotor threads, improving lifetime and reducing maintenance. Additionally, the magnetic coupling provides an intrinsic overload protection mechanism, as forces saturate instead of causing mechanical failure, making MLS devices suitable for safety-critical or high-shock operating environments. Several studies have investigated how magnet geometries, magnetisation patterns, and magnetic circuit materials affect the performance of MLS devices [5, 6]. More advanced solutions introduced Halbach arrays, which enhance air-gap flux density by redirecting magnetic flux towards the active region [7]. However, a full Halbach array implementation in a helical form is notably difficult to manufacture due to magnetisation constraints, complex geometry, and assembly challenges. As a result, research has shifted towards configurations, where discrete PMs are used [8, 9]. These configurations offer improved controllability of the magnetic field while remaining feasible to fabricate.

In parallel with magnetisation optimisation, material selection for the MLS rotor plays a critical role in determining flux density, pull-out force, and magnetic losses. Conventional rotors made from solid steels such as AISI 1020 exhibit high permeability but suffer from significant eddy-current losses, particularly at higher

speeds. Recent advances in SMCs have opened the possibility of using materials with 3D isotropic magnetic properties and substantially reduced eddy-current losses due to their electrically insulating granulated structure [10]. Their lower permeability can reduce force capability, but their manufacturability and magnetic loss benefits may outweigh this drawback in many applications.

This context highlights the need for MLS designs that combine feasible Halbach-like magnetisation patterns with material solutions that balance flux capability and magnetic losses. Yet, studies analysing the performance impact of quasi-Halbach arrays together with SMC-based rotors remain limited. Most prior work either focuses solely on magnetisation geometry or evaluates MLS structures with conventional steel rotors. A comprehensive comparison that includes prototype validation was not found in the literature.

This paper presents a novel MLS topology employing a helically arranged quasi-Halbach array on the slider to enhance air-gap flux density without relying on impractical ideal Halbach magnetisation patterns. Second, it evaluates the use of a SMC rotor, enabling better manufacturability and the potential for lower magnetic losses relative to solid steel. Third, the study provides a combined finite element and experimental assessment comparing SMC and steel rotors, offering a complete design-to-prototype validation. The results show significant gains in pull-out force and specific force per magnetic material volume, demonstrating the practical advantage of the proposed arrangement.

2 | Topology and Analysis

The proposed topology relies on the concept of a quasi-Halbach array applied to the MLS. It is implemented with four magnetisation orientations, i.e., two radial and two axial directions. The presence of the radial components distinguishes it from the purely axial array, which contains only two axially oriented sets of PMs [4, 11]. The performance of the MLS with two different materials for the rotors is also investigated.

2.1 | Topology of the MLS

To evaluate the proposed magnetic topology, the study compares an MLS with axially oriented NdFeB-type PMs to its quasi-Halbach array counterpart. Both devices are modelled with the same dimensions, gear ratio G, and grade of the hard magnetic materials. The quasi-Halbach configuration uses discretized NdFeB-type pieces to form the array, as shown in Figure 1(a). The axially oriented array configuration has a slider with a PM array using steel pieces between adjacent PMs with different polarities, as shown in Figure 1(b). This is considered only theoretically and for the purpose of comparison.

The design of the MLS was aided by the use of the ANSYS magneto static optimetrics tools.

2.2 | Magnetic Materials

A rotor made of SMC, called Somaloy Prototyping Material (SPM) and provided by Höganäs AB [12], in the form of radial discs,

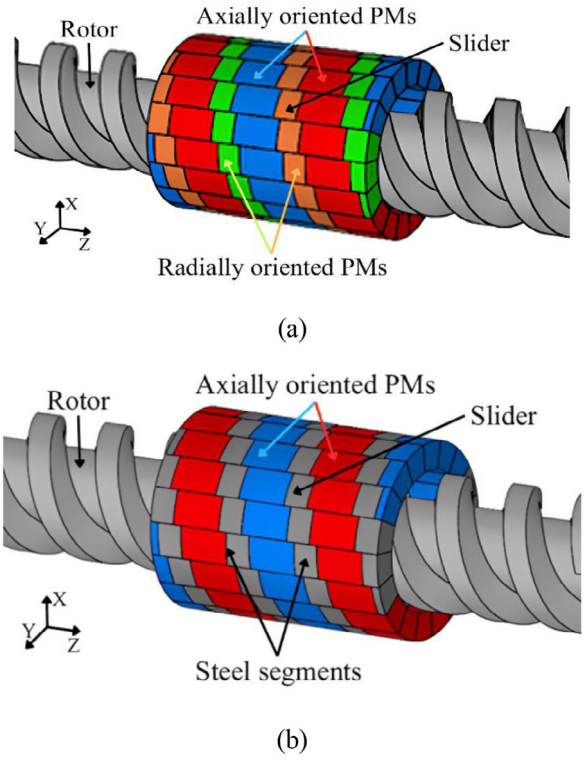

FIGURE 1 | 3D model view of the MLSs: (a) quasi-Halbach array; and (b) axial array.

TABLE 1 | Magnetic properties for materials used.

Magnetic quantities	SPM	AISI 1020 steel
B	1.46 T	1.83 T
μ_r	430	568

is investigated. By doing this, construction issues related to the helical shape were addressed since the SPMs are supplied in a disc format, which is axially small.

The SMC has lower magnetic permeability than AISI 1020 steel. This can result in a lower air-gap flux density and, consequently, a reduced pull-out force. However, it can reduce eddy current losses in the rotor when compared to a solid steel one. Conversely, the latter can produce a larger pull-out force under the same dimensions of the magnetic circuit in both cases.

The magnetic saturation must be considered when seeking to maximize the axial force per volume since it affects the air-gap flux density. To deal with this and based on a set of numerical analyses, the rotor was designed with a trapezoidal thread screw. Table 1 shows the magnetic properties of the SPM and AISI 1020 steel as used in this work. The magnetic flux density, B, corresponds to a magnetic field intensity $H = 10$ kA/m based on [13, 14].

N50 grade PMs were selected and characterised by the authors at a temperature of 25°C. The main PM parameters to consider in this case are the remanent magnetic flux density $B_r = 1.38$ T, the coercivity $H_c = 1037$ kA/m, and the maximum energy product

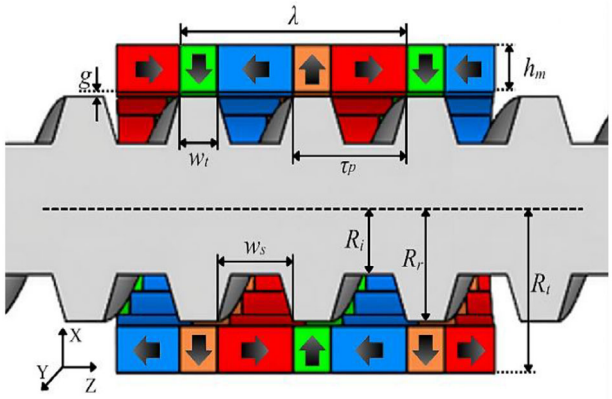

FIGURE 2 | Axial cut view of the MLS with dimensional parameters.

TABLE 2 | Dimensional parameters for the prototypes.

Symbol	Parameter	Value
w_t	Thread width	9 mm
w_s	Slot width	18 mm
τ_p	Pole pitch	27 mm
λ	Lead	54 mm
G	Air-gap height	1 mm
h_m	Magnet height	10 mm
P	Poles	2
R_i	Rotor internal radius	14 mm
R_r	Rotor external radius	24 mm
R_t	Slider external radius	35 mm

$BH_{max} = 404$ kJ/m^3. For the study of an MLS, the mechanical and magnetic features are dependent on the physical characteristics and dimensions of the model. The dimensional variables of the MLS are given in Figure 2 and tabulated in Table 2.

Once the slider comprehends the set of PMs, the key design variables are the height of the magnets and the axial length of the radial and axial magnets, which are compatible with the axial length of the slot and thread in the rotor, respectively.

For the rotor, the main dimensional design variables are the pole pitch and the rotor radius, which define the inclination of the screw thread. The pole pitch is defined as the sum of the axial lengths of the thread and the slot. With the definition of the pole pitch, the gear ratio G is

$$G = \frac{\omega}{v} = \frac{F}{T} = 2\pi / ((w_t + w_s) P) \quad (1)$$

where ω represents the angular speed [rad/s] of the rotor, v is the corresponding linear speed [m/s] of the slider, F is the axial force, and T is the consequent torque. Applied to the configuration under study, it gives $G = 116.4$ rad/m.

Difficulties arise when trying to create an ideal spiral with the PMs for the slider, such as complications with the magnetisation, the assembly, and even the machining process. A practical solution involves discretizing the spiral into segments of PMs, as suggested by Ling et al. [9]. The latter demonstrates that using a discretization of the PMs with smaller pieces can produce a good approximation of an ideal spiral as far as the MLS is concerned. For this prototype, a 20 degrees arc segment for the discretized PMs was adopted, i.e., one turn requires eighteen pieces of PMs pieces.

2.3 | FEA

For this study, a FEA was performed using the ANSYS Electronics software to provide theoretical results. The model considered the magnetic flux density with attention to the concentration points to avoid saturation and the maximum pull-out axial force and torque produced. Simulation results were obtained for the 3D models of both topologies, i.e., axial array and a quasi-Halbach array, as illustrated in Figure 1, using a 3D model that accounted for the proper characteristics of the magnetic materials. There were four simulation models involving the two topologies, each one using the two rotors one at a time with different soft magnetic materials.

The design of the trapezoidal thread adopts a tooth angle of 35.6°, which contributes to reducing the magnetic saturation at its edges.

3 | Prototype

To obtain experimental results, a prototype using a slider that matches the quasi-Halbach array, guiding rails and bearings, and an external case was assembled. It allows the use of two threaded rotors: one with SPM and another made from AISI 1020 steel.

SMC has a lower maximum magnetic permeability, which can reduce the resulting air-gap flux density and, consequently, the axial force. However, the material can also reduce eddy-current losses in the rotor when compared to a solid steel rotor, as already mentioned.

The composite rotor is constructed from stacked discs of SPM glued together to form a rigid rod, as shown in Figure 3(a), which is machined in order to produce the rotor thread. The thread machining process was carried out using a CNC machine and resulted in the final rotor form presented in Figure 3(b).

The steel rotor thread was machined from a rigid rod of AISI 1020 steel as shown in Figure 4.

The slider is constructed from an aluminium case with internal dovetail joints that hold the PMs in place. These are arranged to form a helix, as shown in Figure 5. This case also allows the mounting of the linear bearings.

After the assembly of the PMs inside the case, the distribution of the slider magnetic flux density was checked using a magnetic viewing film. Figure 6 shows the expected helix pattern.

To build the system, linear guides, axis guides, and an external cylinder are added to keep the parts together, as illustrated in Figure 7. The total mass of the slider moving parts is 3.9 kg.

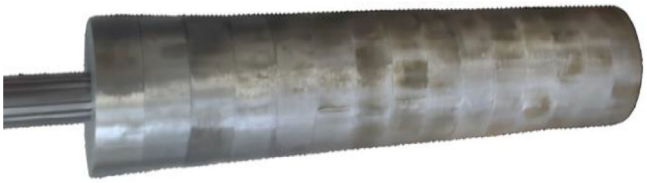

(a)

(b)

FIGURE 3 | The SPM rotor: (a) glued discs and axis; and (b) machined trapezoidal thread.

FIGURE 4 | The AISI 1020 steel rotor with trapezoidal thread.

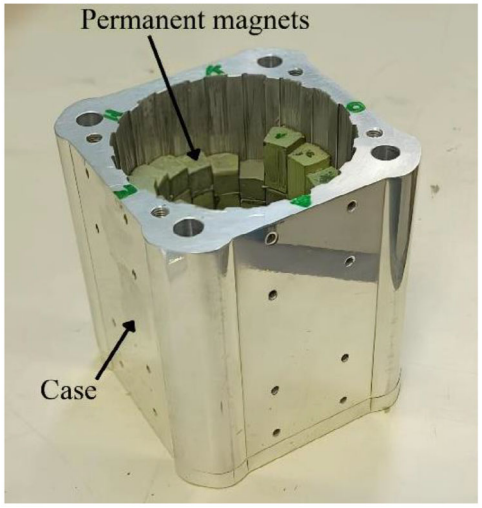

FIGURE 5 | The slider with some PM pieces assembled inside.

4 | Tests and Results

The pull-out force numerical results were computed by means of the FEA model using the relative slider axial position with respect to the rotor as the variable parameter. Once the rotor position is fixed, a step-by-step variation of position of the slider position misalignment with respect to the rotor thread takes place, and the pull-out force calculated.

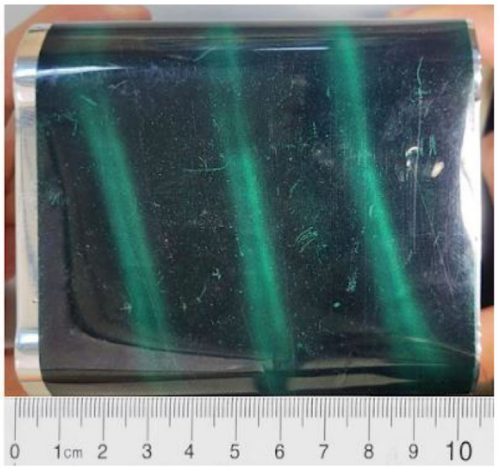

FIGURE 6 | Slider with a magnetic viewing film placed around the former.

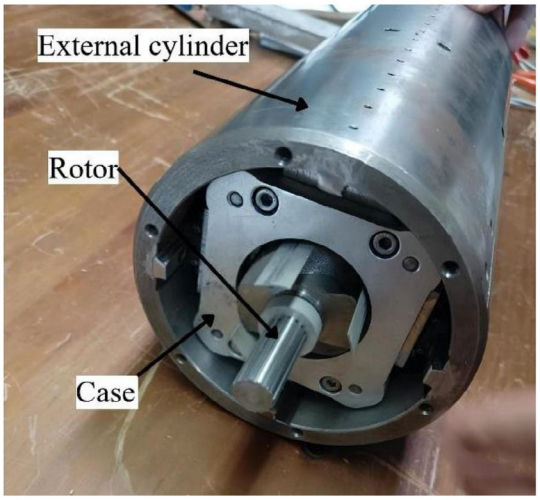

FIGURE 7 | The external cylinder with the rotor allocated inside the slider.

This allows the computation of the pull-out axial force and torque. The same methodology was applied to the experimental measurement procedure, which is similar to [7] and is performed in a static fashion.

To compare with the numerical results, the quasi-Halbach array configuration prototype, either using the SPM rotor or the steel rotor, was tested on an MTS 810 servo-hydraulic material testing system with a load cell able to measure up to 500 kgf with 0.5% rated error. To obtain the pull-out axial force, the rotor was locked. The test machine imposes a controlled axial displacement on the slider, and as the load cell is attached to the axis guides, the force is measured according to the setup shown in Figure 8. Table 3 shows FEA and experimental results. The maximum pull-out axial force obtained from the FEA with the SPM rotor is 1.1674 kN with the axial array version, while the quasi-Halbach array version goes up to 1.9057 kN, i.e., a 63.2% difference that favours of the latter.

Based on those results, Table 4 shows the calculated maximum pull-out force per unit of volume of the PMs and per active

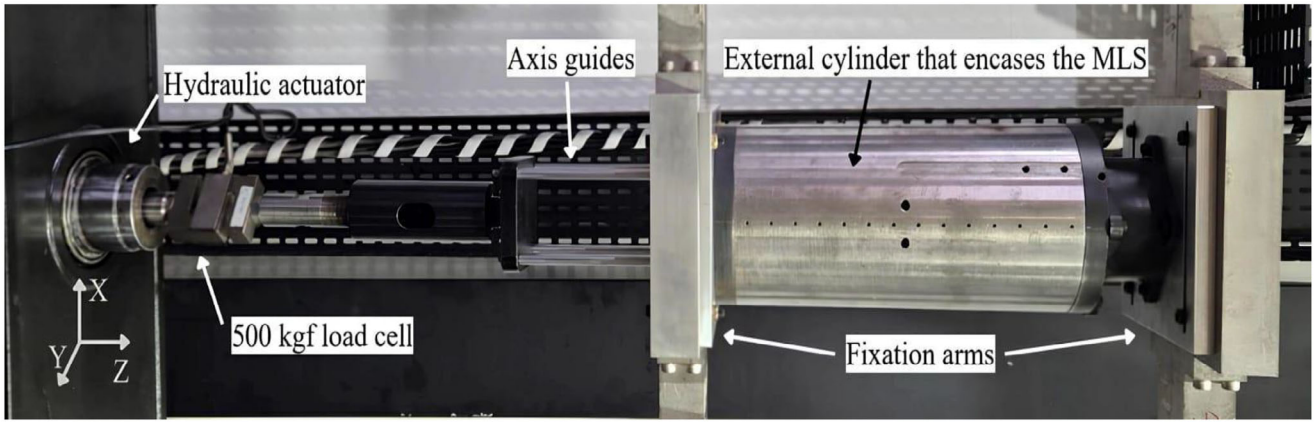

FIGURE 8 | With quasi-Halbach array and SMC rotor under test by the MTS 810 machine.

TABLE 3 | Measured pull-out force and torque of the MLS with quasi-Halbach array and FEA pull-out force and torque for quasi-Halbach and axial arrays.

Prototype	Configuration	Pull-out force (N)	Pull-out torque (Nm)
Quasi-Halbach array MLS	Experimental SPM rotor	1710.8	14.7
	Experimental AISI 1020 steel rotor	1820.4	15.6
	FEA SPM rotor	1905.7	16.4
	FEA AISI 1020 steel rotor	2040	17.5
Axial array MLS	FEA SPM rotor	1167.4	10.0
	FEA AISI 1020 steel rotor	1250.2	10.7

TABLE 4 | Maximum pull-out force and torque analysis per volume.

Quasi-Halbach array MLS—permanent magnets volume 169.6 cm^3—active volume 346.4 cm^3					
Axial array MLS—permanent magnets volume 113.1 cm^3—active volume 346.4 cm^3					
Prototype	**Configuration**	**Maximum pull-out force**		**Maximum pull-out torque**	
		Per volume of permanent magnets (N/cm^3)	**Per slider active volume (N/cm^3)**	**Per volume of permanent magnets (Nm/cm^3)**	**Per slider active volume (Nm/cm^3)**
Quasi-Halbach array MLS	Experimental SPM rotor	10.08	4.94	0.087	0.042
	Experimental AISI 1020 steel rotor	10.73	5.26	0.092	0.045
	FEA SPM rotor	11.24	5.49	0.097	0.047
	FEA AISI 1020 steel rotor	12.02	5.89	0.103	0.051
Axial array MLS	FEA SPM rotor	10.32	3.37	0.088	0.029
	FEA AISI 1020 steel rotor	11.05	3.61	0.095	0.031

volume. The latter is defined as the sum of the permanent-magnets volume, the slider's ferromagnetic material for the axial array configuration, the rotor portion magnetically coupled to the slider, and the air-gap between slider and rotor.

The results for the SPM rotor in terms of pull-out force as a function of the axial displacement of the slider with locked rotor are presented in Figure 9. For the steel rotor, Figure 10 shows the results.

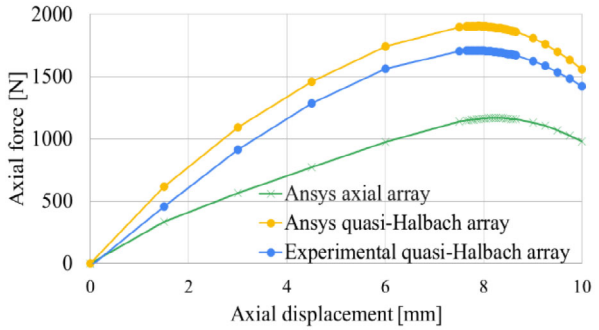

FIGURE 9 | Pull-out force due to slider axial displacement with blocked SPM rotor.

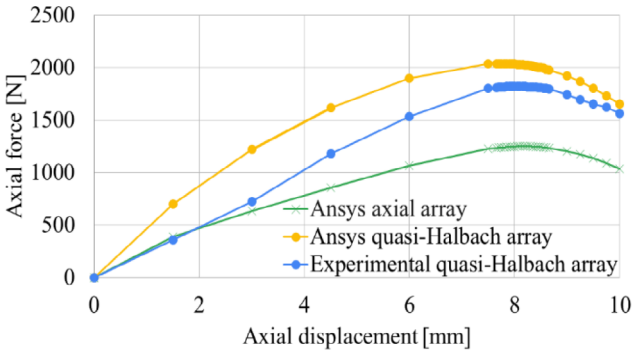

FIGURE 10 | Pull-out force due to slider axial displacement with blocked AISI 1020 steel rotor.

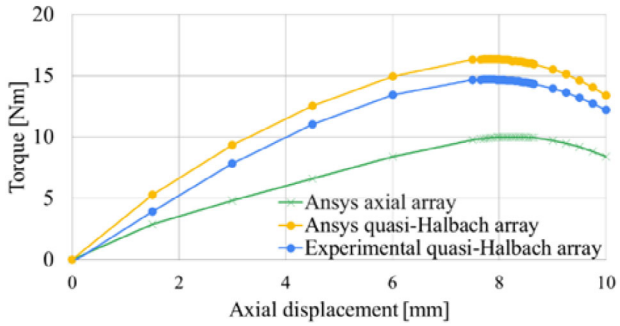

FIGURE 11 | Pull-out torque due to slider axial displacement with blocked SPM rotor.

And the results for the SPM and steel rotors in terms of pull-out torque as a function of the axial displacement of the slider with locked rotor are presented in Figures 11 and 12, respectively.

5 | Conclusion

This work presents a novel topology for a MLS that utilises a slider composed of a helically arranged quasi-Halbach array of PMs and a rotor made of SMC. The key aspects of the prototype were discussed, along with FEA and experimental results, demonstrating significant improvements when using quasi-Halbach arrays compared to axial arrays. The FEA results in terms of pull-out force and torque demonstrate that quantities achieve higher

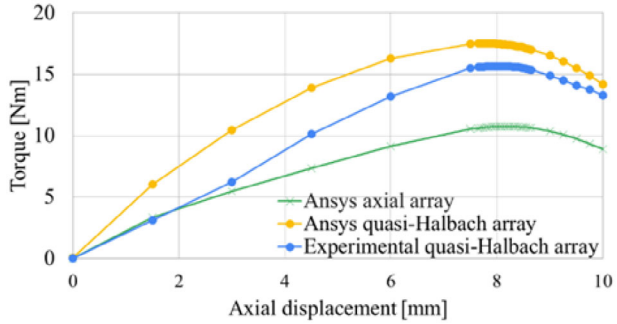

FIGURE 12 | Pull-out torque due to slider axial displacement with blocked AISI 1020 steel rotor.

values for the quasi-Halbach MLS when compared to the axial array version, and the experimental results corroborate these findings as demonstrated by the results in Tables 3 and 4.

By using different materials for the rotor, i.e., SPM and AISI 1020 steel, it is shown that there is an increase in pull-out force per slider active volume with the quasi-Halbach array version in terms of experimental results: the MLS prototype with the SPM rotor achieved a 46.5% increase when compared to its theoretical axial array version. The MLS with an AISI 1020 steel rotor achieved a 45.6% increase when compared to its axial array. The AISI 1020 steel rotor produced a nearly 6% larger force and torque due to higher magnetic permeability compared with the SPM (Table 1), which allows a higher air-gap magnetic flux density.

The feasibility of using a soft magnet composite to form the rotor of the MLS is promising, despite producing slightly lower pull-out force and torque. However, its real advantage must be verified in terms of magnetic losses as a function of the linear speed for both rotors in future work. This work contributes to an original way to use a SMC to create a rotor that produces reasonable results and enables a study of its magnetic losses.

Author Contributions

Aly Flores Filho: conceptualization, data curation, formal analysis, funding acquisition, investigation, methodology, supervision, validation, writing – original draft. **Paulo Eckert:** funding acquisition, project administration, supervision, validation, writing – review & editing. **David Dorrell:** data curation, validation, writing – review & editing. **Davi Bertele:** investigation, methodology, validation, visualization, writing – original draft. **Lucas Vinskoski:** formal analysis, investigation, methodology, visualization, writing – original draft.

Acknowledgements

This work was supported by the Fundacao de Desenvolvimento da Pesquisa (FUNDEP) through the Rota 2030/Linha V grant number 27192.03.02/2021.02.00, and by the National Council for Scientific and Technological Development (CNPq) grant numbers 303643/2023-4, 306166/2021-6 and 310375/2025-8. The authors would also like to thank Höganäs AB for donating the SMC used to fabricate the rotor.

Conflicts of Interest

The authors declare no conflicts of interest.

Data Availability Statement

The data that support the findings of this study are available from the corresponding author upon reasonable request.

References

1. A. Zhao, W. Wu, J. Jiang, L. Zhu, and K. Lu, "Design and Experiment of a Magnetic Lead Screw for the Point-Absorbing Wave Energy Conversion System," *IET Electric Power Applications* 14, no. 11 (2020): 2146–2153, https://doi.org/10.1049/iet-epa.2019.0486.

2. F. Gao, Q. Wang, and J. Zou, "Comparison and Optimization of a Magnetic Lead Screw Applied in a Wave Energy Converter," *Electronics* 11, no. 18 (2022): 2825, https://doi.org/10.3390/electronics11182825..

3. M. B. Kouhshahi, J. Z. Bird, J. D. Kadel, and W. B. Williams, "Designing and Experimentally Testing a Magnetically Geared Lead Screw," *IEEE Transactions on Industry Applications* 54, no. 6 (2018): 5736–5747, https://doi.org/10.1109/TIA.2018.2846651.

4. M. Cirolini, A. F. Flores Filho, Y. C. Wu, and D. G. Dorrell, "Design Aspects of a Reluctance-Based Magnetic Lead Screw," *IEEE Transactions on Magnetics* 55, no. 7 (2019): 1–6, https://doi.org/10.1109/TMAG.2019.2895681.

5. D. Mustafa and H. A. Hussain, "A Review and Comparative Study on the Design and Analysis of Magnetic Lead Screws," *IEEE Transactions on Industry Applications* 59, no. 4 (2023): 4108–4119, https://doi.org/10.1109/TIA.2023.3270270.

6. Q. Wang, F. Gao, J. Zhang, and Y. Li, "Analysis and Reduction of Detent Effect in Magnetic Lead Screws With Parallel Magnetized Permanent Magnet Segments," *IEEE Access* 8 (2020): 84177–84187, https://doi.org/10.1109/ACCESS.2020.2991786.

7. N. Bianchi and E. Fornasiero, "A Novel Analytical Formulation of the Magnetic Field Distribution in Halbach Array Surface PM Machines," *Magnetism* 3, no. 4 (2023): 280–296, https://doi.org/10.3390/magnetism3040022.

8. D. Mustafa, H. A. Hussain, and H. A. Toliyat, "Design and Analysis of Discrete Halbach Magnetic Lead Screws Using Nonskewed PMs," *IEEE Transactions on Transportation Electrification* 11, no. 2 (2024): 5434–5444, https://doi.org/10.1109/TTE.2024.3481243.

9. Z. Ling, W. Zhao, J. Ji, and G. Liu, "Design of a New Magnetic Screw With Discretized PMs," *IEEE Transactions on Applied Superconductivity* 26, no. 4 (2016): 0602805, https://doi.org/10.1109/TASC.2016.2536651.

10. H. Shokrollahi and K. Janghorban, "Soft Magnetic Composite Materials (SMCs)," *Journal of Materials Processing Technology* 189, no. 1–3 (2007): 1–12, https://doi.org/10.1016/j.jmatprotec.2007.02.034.

11. M. Cirolini, A. F. Flores Filho, P. R. Eckert, and L. D. C. Franchi, "Realizing and Experimentally Testing a Reluctance-Based Magnetic Lead Screw", in *19th International Symposium on Electromagnetic Fields, (ISEF)* (2019): 1–2, https://doi.org/10.1109/ISEF45929.2019.9097079.

12. A. B. Höganäs, 'Somaloy Prototyping Material, SPM', April 2016, [Online]. Available: https://www.hoganas.com/globalassets/downloads/libary/somaloy_prototyping-material_1334hog.pdf, accessed 12 December 2025.

13. A. Drehmer, G. J. L. Gerhardt, and F. P. Missell, "Case Depth in SAE 1020 Steel Using Barkhausen Noise," *Materials Research* 16, no. 5 (2013): 1015–1019, https://doi.org/10.1590/S1516-14392013005000095.

14. T. Tadic and B. G. Fallone, "Design and Optimization of Superconducting MRI Magnet Systems With Magnetic Materials," *IEEE Transactions on Applied Superconductivity* 22, no. 2 (2012): 4400107, https://doi.org/10.1109/TASC.2012.2183871..